Research Article | Vol. 32, No. 9 / 22 Apr 2024 / Optics Express 15093

Optics EXPRESS

Upconversion-pumped femtosecond thulium laser at 2309 nm mode-locked by a GaSb-based SESAM

ALEKSEY TYAZHEV,[1] JI EUN BAE,[2] MARCO GAULKE,[3] PAVEL LOIKO,[2] JONAS HEIDRICH,[3] MATTHIAS GOLLING,[3] SAID IDLAHCEN,[1] LAUREN GUILLEMOT,[2] THOMAS GODIN,[1] PATRICE CAMY,[2] URSULA KELLER,[3] AND AMMAR HIDEUR[1,*]

[1] *CORIA UMR6614, CNRS-INSA-Université de Rouen, Normandie Université, Avenue de l'université, BP. 12, 76801 Saint Etienne du Rouvray, France*
[2] *Centre de Recherche sur les Ions, les Matériaux et la Photonique (CIMAP), UMR 6252 CEA-CNRS-ENSICAEN, Université de Caen Normandie, 6 Boulevard Maréchal Juin, 14050 Caen Cedex 4, France*
[3] *ETH Zurich, Department of Physics, Institute for Quantum Electronics, Auguste-Piccard-Hof 1, Zurich 8093, Switzerland*
[*] *hideur@coria.fr*

Abstract: We report on a femtosecond thulium laser operating on the $^3H_4 \rightarrow {}^3H_5$ transition with upconversion pumping around 1 µm and passively mode-locked by a GaSb-based SEmiconductor Saturable Absorber Mirror (SESAM). This laser employs a 6 at.% Tm:$LiYF_4$ laser crystal and a polarization maintaining Yb-fiber master oscillator power amplifier at 1043 nm as a pump source addressing the $^3F_4 \rightarrow {}^3F_{2,3}$ excited-state absorption transition of Tm^{3+} ions. In the continuous-wave regime, the Tm-laser generates 616 mW at ~2313 nm with a slope efficiency of 10.0% (vs. the incident pump power) and a linear polarization (π). By implementing a type-I SESAM with a single ternary strained $In_{0.33}Ga_{0.67}Sb$ quantum well embedded in GaSb for sustaining and stabilizing the soliton pulse shaping, the self-starting mode-locked Tm-laser generated pulses as short as 870 fs at a central wavelength of 2309.4 nm corresponding to an average output power of 208 mW at a pulse repetition rate of 105.08 MHz and excellent mode-locking stability. The output power was scaled to 450 mW at the expense of a longer pulse duration of 1.93 ps. The nonlinear parameters of the SESAM are also reported.

1. Introduction

Laser sources emitting around 2.3 µm find applications in gas sensing and pollutant detection [1,2], combustion studies [3] and non-invasive glucose blood measurements [4] and they are also noteworthy for pumping of mid-infrared optical parametric oscillators [5]. This spectral range can be addressed by several types of laser sources. Chromium ions (Cr^{2+}) in zinc chalcogenides (ZnS, ZnSe) offer extremely broad emission bands leading to broadband wavelength tuning and generation of femtosecond pulses [6,7]. However, the synthesis of these gain media of high optical quality is challenging and they suffer from moderate laser-induced damage thresholds and the need of special pump sources (Er-fiber lasers or semiconductor diode lasers [8]). Another possibility constitutes Vertical-Cavity Surface-Emitting Lasers (VCSELs) employing semiconductor heterostructures (GaInAs on InP or GaInAsSb on GaSb) however with very limited output powers [9,10]. As shown recently, optically pumped Vertical-External-Cavity Surface-Emitting Lasers (VECSELs) feature better power scaling capabilities and enable femtosecond pulse generation at high repetition rates [11]. Another solution is the use of bulk and fiber thulium (Tm^{3+}) lasers operating on the $^3H_4 \rightarrow {}^3H_5$ electronic transition, Fig. 1 [12,13]. Although this

#516958 https://doi.org/10.1364/OE.516958
Journal © 2024 Received 22 Dec 2023; revised 20 Feb 2024; accepted 28 Feb 2024; published 9 Apr 2024

laser scheme has been known for a long time, there has been growing interest in such sources over the past decade due to the availability of both laser gain media (Tm^{3+}-doped fluoride crystals and glasses) and pump sources (AlGaAs laser diodes emitting at ~0.8 µm).

The power scaling capabilities and the proof-of-principle of highly efficient laser operation of continuous-wave (CW) Tm-lasers operating on the $^3H_4 \rightarrow {}^3H_5$ transition were recently demonstrated. Guillemot *et al*. reported on a $Tm:KY_3F_{10}$ laser delivering 0.84 W at 2.34 µm with a slope efficiency of 47.7% (under pumping by a Ti:Sapphire laser) [14]. Loiko *et al.* has shown that the slope efficiency for 2.3-µm Tm-lasers can exceed the Stokes limit owing to the positive effect of energy-transfer upconversion (ETU) from the terminal laser level, $^3F_4 + {}^3F_4 \rightarrow {}^3H_4 + {}^3H_6$, refilling the upper laser manifold and boosting the pump quantum efficiency up to 2 (a two-for-one pump process) [15,16]. In their early study, Pinto *et al.* achieved continuous wavelength tuning of a $Tm:LiYF_4$ laser across a broad range of 2.20–2.46 µm [17]. Recently, Yu *et al*. has presented a diode-pumped $Tm:GdVO_4$ laser scaled to the multi-watt output power level (>6 W at 2.29 µm) representing a record-high output from this type of sources reported to date [18].

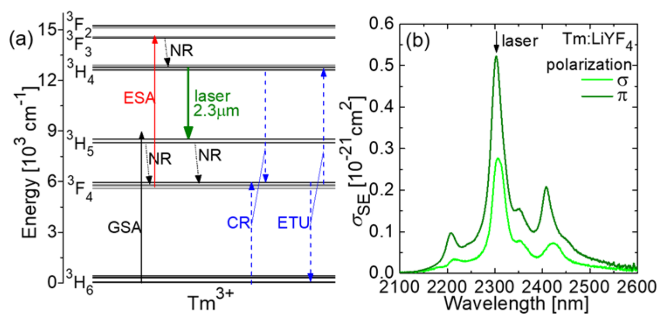

Fig. 1. (a) A partial energy-level scheme of Tm^{3+} ions in $LiYF_4$ [23] illustrating the upconversion pumping scheme for the $^3H_4 \rightarrow {}^3H_5$ laser transition: GSA / ESA – ground / excited state absorption, CR – cross-relaxation, ETU – energy-transfer upconversion, *green arrow* – laser transitions, NR – multiphonon non-radiative relaxation; (b) stimulated-emission cross-sections, σ_{SE}, for the $^3H_4 \rightarrow {}^3H_5$ Tm^{3+} transition in $LiYF_4$ for π and σ light polarizations, *arrow* indicates the laser wavelength.

The first mode-locked 2.3-µm Tm-laser was reported in 2017 by Soulard *et al.* [19] using a commercial SEmiconductor Saturable Absorber Mirror (SESAM) comprising the $In_xGa_{1-x}As$ quantum well (QW) technology and a $Tm:LiYF_4$ laser crystal: 94 ps-long pulses were generated at 2306 nm with an average output power of 165 mW at a repetition rate of ~100 MHz. In the study by Kowalczyk *et al.* [20], the negative etalon effect of the SESAM substrate in the inverted geometry was identified to modulate the laser spectrum and limit the pulse duration to ~100 ps. Furthermore, in 2017, Canbaz *et al.* presented a femtosecond Kerr-lens mode-locked $Tm:LiYF_4$ laser that generated 514-fs pulses at 2303 nm, albeit with a very low average output power of 14.4 mW at 41.5 MHz [21]. Subsequently, the same group of authors further developed $Tm:LiYF_4$ and $Tm:KY_3F_{10}$ lasers passively mode-locked by graphene saturable absorbers, achieving slightly longer pulses but still at low average output powers [22]. Note that all these oscillators were pumped by Ti:Sapphire lasers at ~0.78 µm (“direct” pumping to the upper laser manifold, $^3H_4$). This naturally limited further development of such sources and their power scalability. Although spatially multimode fiber-coupled AlGaAs laser diodes are available, their use in pumping mode-locked laser cavities is limited. This limitation is due to low brightness, expected poor mode-matching efficiency, severe thermal problems, and low associated laser efficiency. Table 1 provides an overview of mode-locked 2.3-µm Tm-lasers reported to date. In the same table, for comparison, we also provide several milestone results on mode-locked lasers employing Cr^{2+}-doped zinc chalcogenides (ZnS and ZnSe).

Table 1. Output Characteristics[a] of Mode-Locked Thulium Lasers at ~2.3 µm Reported So Far. Selected Results on Mode-Locked Cr^{2+}-Ion Lasers are Given for Comparison

Material	SA[b]	P_{out}, W	λ_L, µm	$\Delta\tau$, ps	PRR, MHz	Ref.
$Tm:LiYF_4$	SESAM	0.165	2.306	94	100	[19]
	KLM	0.014	2.303	0.514	41.5	[21]
	Graphene	0.042	2.304	0.921	17.2	[22]
	SESAM	**0.208**	2.309	**0.870**	105.1	This work
		0.450	2.306	1.93	114.5	This work
$Tm:KY_3F_{10}$	SESAM	0.090	2.340	~100	107.4	[20]
	Graphene	0.064	2.340	0.739	54	[22]
Cr:ZnS	SESAM	0.8	2.370	0.079	250	[6]
	KLM	0.25	2.325	0.044	78.9	[7]
Cr:ZnSe	KLM	0.5	2.420	0.043	83	[7]

[a] P_{out} – average output power, λ_L – laser wavelength, $\Delta\tau$ – pulse duration, PRR – pulse repetition rate.
[a] SESAM – SEmiconductor Saturable Absorber Mirror, KLM – Kerr-lens mode-locking.

Recently, an original upconversion (UC) pumping scheme for Tm^{3+} ions was proposed with a goal of replacing Ti:Sapphire lasers as pump sources. It is based on a weak non-resonant ground-state absorption (GSA) $^3H_6 \to {}^3H_5$ followed by a non-radiative step down to the $^3F_4$ metastable state, as well as a resonant $^3F_4 \to {}^3F_{2,3}$ excited-state absorption (ESA) [23], Fig. 1. This scheme is driven by a photon avalanche mechanism [24] involving a cross-relaxation process among adjacent Tm^{3+} ions, $^3H_4 + {}^3H_6 \to {}^3F_4 + {}^3F_4$, recirculating the populations between the ground and metastable Tm^{3+} manifolds. The ESA transition of interest can be addressed by Yb-fiber lasers (YFLs) emitting slightly above 1 µm. The YFL technology combines the inherent advantages of fiber lasers, such as small footprint, flexible design, and high-power operation enabled by distributed heat management with good beam quality (high-brightness sources). Additionally, the characteristics of ytterbium (Yb^{3+}) ions are beneficial, including a simple energy-level scheme leading to high laser efficiencies and weak heat loading. Furthermore, the large Stark splitting of the ground state in ytterbium ions enables broadband wavelength tunability around 1 µm. This tunability is crucial for addressing the very intense but narrow ESA peaks of Tm^{3+} ions within this spectral range.

Tyazhev *et al.* fully exploited this approach to demonstrate the first watt-level Tm-fiber laser at 2.3 µm with upconversion pumping enabled by a 1049-nm YFL. In the CW regime, the Tm:ZBLAN fiber laser delivered 1.24 W at 2.27 µm with a slope efficiency of 37% [25]. UC pumping has been employed in various bulk Tm-lasers using both fluoride and oxide crystals [26–28]. However, the output powers remained limited, raising questions about the viability of this approach for these types of laser sources. Dupont *et al.* proposed a modification of this pumping scheme via dual-wavelength pumping to initiate pump absorption from the metastable $^3F_4$ Tm^{3+} manifold, but this resulted in only an incremental power improvement [29]. To date, no mode-locked Tm-lasers with UC pumping have been reported.

SESAM mode-locking offers several advantages. SESAMs are widely known for enabling reliable self-starting mode-locked lasers and for their use in robust laser cavities that operate effectively in the middle of their stability zones [30]. They can support high average output powers. Compared to physical saturable absorbers like nanomaterials (e.g., graphene), SESAMs have several benefits: they are commercially available, have a robust and solid design, offer better uniformity, and present a lower risk of degradation under environmental conditions and during laser operation. Furthermore, they allow for more precise design of their nonlinear optical properties, albeit within somewhat narrower operation ranges. In particular, SESAMs based on $In_xGa_{1-x}As$ quantum wells (QWs) have revolutionized the field of ultrafast oscillators in the near-infrared by solving the Q-switching instability problem [31]. However, their applications in the short-wave infrared spectral range remain limited.

In this spectral range, gallium antimonide (GaSb) offers a promising alternative [32]. The high refractive index difference of GaSb and AlAsSb enables fabrication of highly reflective distributed Bragg reflectors (DBRs) with wide stop bands. The bandgap in InGaAsSb QWs can be tailored to address laser wavelengths ranging from 1.9 µm to beyond 3 µm. The InGaAsSb Auger recombination rate increases significantly above 2 µm, making the SESAM recovery dynamics extremely fast with sub-ps recovery times [33]. In this case, no defect engineering is required to reduce the recovery time as in the case of $In_xGa_{1-x}As$ QWs. Recently, GaSb-based SESAM has been actively studied regarding their ultrafast nonlinear properties and femtosecond mode-locked laser performance in the spectral ranges around 2 µm [34,35] and 2.4 µm [6,8,36]. Barh *et al.* reported on a GaSb-based SESAM mode-locked Cr^{2+}:ZnS laser generating 79 fs pulses at 2.37 µm with a watt-level average output power at a high repetition rate of ~250 MHz [6]. Single-cavity dual-modelocked Cr^{2+}:ZnS laser employing a GaSb-based SESAM has been reported also recently [36].

In the present work, we report on the first passively mode-locked thulium laser operating on the $^3H_4 \rightarrow {}^3H_5$ transition with upconversion pumping. A GaSb-based SESAM was used to initiate and stabilize the mode-locked operation.

2. GaSb-based SESAM

The saturable absorber was a GaSb-based SESAM (ETH Zürich) with a single ternary strained InGaSb quantum well (QW, 16 nm, 33% In) embedded in GaSb, Fig. 2. It thus had a type-I configuration with a potential well for holes and electrons existing in same material layer leading to high Auger recombination rate. The SESAM structure contained a highly reflective distributed Bragg reflector (DBR) consisting of 24 lattice-matched high- and low-index layer pairs ($AlAs_{0.08}Sb_{0.92}$/GaSb) on a GaSb substrate and an absorber region of single $In_{0.33}Ga_{0.67}Sb$ QW embedded in GaSb on top of the DBR structure grown by molecular beam epitaxy (MBE) [32]. The high reflectivity with small non-saturable losses in this SESAM results in a standing-wave electric-field intensity pattern with well-defined nodes and antinodes as shown in Fig. 2.

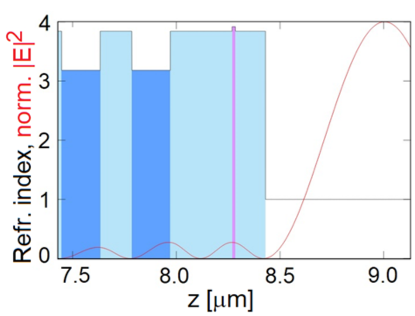

Fig. 2. Design of the single-quantum-well GaSb-based SESAM: refractive index profile (*light blue* – GaSb, *dark blue* – $AlAs_{0.08}Sb_{0.92}$, *pink* – $In_{0.33}Ga_{0.67}Sb$ (QW), *red curve* –electric field intensity normalized to 4 in air plotted over the thickness of the structure, where z is the distance from the GaSb substrate perpendicular to the QW layers.

The measured low intensity spectral reflectance of the SESAM exhibited a broad stopband exceeding 200 nm centered around 2.3 µm. To accurately characterize the SESAM's nonlinear optical performance, which features low-loss and ultrafast response, the full optical characterization setup described in [37] was employed at the central wavelength of 2.35 µm. The nonlinear reflectivity curve measured using 100 fs-long pulses is shown in Fig. 3(a). This curve was fitted using a rate equation model for a two-level system, assuming a Gaussian beam profile.

$$R(F_\mathrm{p}) = \frac{1}{2F_\mathrm{P}} \int_0^{2F_\mathrm{p}} R_\mathrm{ns} \frac{\ln\left(1 + \left(\frac{R_\mathrm{lin}}{R_\mathrm{ns}}\right)(\exp(F/F_\mathrm{sat}) - 1)\right)}{F/F_\mathrm{sat}} \exp\left(-\frac{F}{F_2}\right) dF, \tag{1}$$

where R is the reflectivity, $F_\mathrm{p} = E_\mathrm{p}/(\pi w^2)$ is the pulse fluence (E_p – pulse energy, w – laser beam radius), F_sat is the saturation fluence, R_lin is the unsaturated reflectivity in the linear regime, R_ns is the highest reflectivity limited by the non-saturable loss, and F_2 is the rollover parameter. The best-fit to the measured nonlinear reflectivity curve yielded the following parameters: F_sat of 21 µJ/cm^2, a modulation depth $\Delta R = R_\mathrm{ns} - R_\mathrm{lin}$ of 0.53%, a non-saturable loss $\Delta R_\mathrm{ns} = 100\% - R_\mathrm{ns}$ of 0.14% and a rollover parameter related to two-photon absorption F_2 of 37 mJ/cm^2, Fig. 3(a). Such low losses facilitate obtaining high average output powers in the mode-locked operation regime. In soliton mode-locked lasers, the SESAM starts and stabilizes the pulse formation, and the latter is further governed by the soliton pulse shaping mechanism [38,39]. The pulse duration is set by the intracavity group-delay dispersion and self-phase modulation (see below).

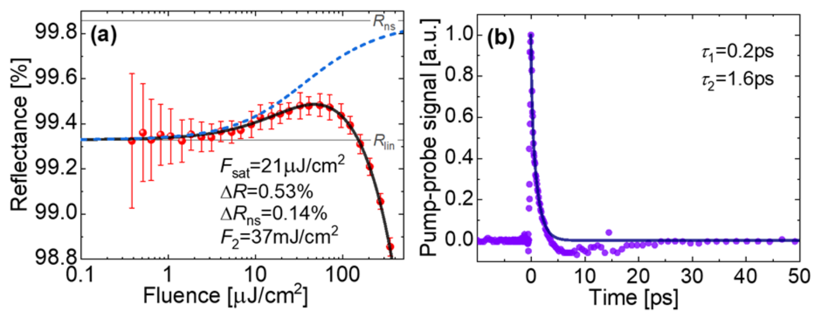

Fig. 3. Characterization of the GaSb-based SESAM: (a) a nonlinear reflectance measurement, *symbols* – experimental data, *curve* – their fit (*black solid*) using Eq. (1), and (*blue dashed*) without rollover effects, *i.e.*, for F_2 = infinity, $\lambda = 2350$ nm; (b) a pump-probe trace, *symbols* – experimental data, *curve* – their biexponential fit using Eq. (2), $\lambda = 2350$ nm.

The pump-probe trace is shown in Fig. 3(b), obtained using a pulse duration of 100 fs and a pump fluence of 17.6 µJ/cm^2. The ultrafast relaxation dynamics of the SESAM were characterized using a bi-exponential decay function:

$$\Delta R(t) = A\mathrm{e}^{-t/\tau_1} + (1 - A)\mathrm{e}^{-t/\tau_2}\ , \tag{2}$$

where ΔR is the change of reflectivity, t is time, A is the weighting constant, and τ_1 and τ_2 are the characteristic recovery times. The best fit using Eq. (2) gave a fast recovery time τ_1 of 0.2 ps with a high weighting constant A of >0.9 and a slow time constant τ_2 of 1.6 ps, which are sufficiently short for stabilizing femtosecond soliton mode-locking [38] in the present work.

3. SESAM mode-locked thulium laser

3.1. Laser set-up

As a gain medium, we employed a 6 at.% $Tm:LiYF_4$ single-crystal grown by the Czochralski (Cz) method under Ar + CF_4 atmosphere. This relatively high Tm^{3+} doping level was selected to ensure sufficient pump absorption under upconversion pumping. A Brewster-cut laser element (thickness: 6.0 mm, aperture: 4.0 × 4.0 mm^2) was oriented for light propagation along the ***a*** crystallographic axis (***a***-cut) for π-polarization. This polarization state gives access to higher ESA cross-sections for the $^3F_4 \rightarrow {}^3F_{2,3}$ pump transition, as well as higher gain for the $^3H_4 \rightarrow {}^3H_5$ laser transition. The laser element was mounted in a Cu-holder cooled by circulating water (18 °C).

The home-made pump source addressing the $^3F_4 \rightarrow {}^3F_{2,3}$ excited-state absorption transition of Tm^{3+} ions (the UC pumping scheme) consisted of a wavelength-tunable Yb-fiber laser, a preamplifier stage and a polarization maintaining large-mode area fiber amplifier featuring a heavily Yb^{3+}-doped fiber with a core diameter of 20 µm (Coherent PLMA-YDF-10/130-VII). The master-oscillator power-amplifier (MOPA) was broadly tunable from 1030 to 1064 nm and delivered up to 8.0 W at 1043 nm with a nearly diffraction limited beam quality ($M^2 \approx 1.1$) and a linear polarization (polarization extinction ratio, PER > 16 dB). High brightness pumping is essential for the development of mode-locked lasers as it enables good overlap between the pump and laser modes (being particularly relevant for long laser crystals), and tight focusing of the pump beam. For the direct pumping scheme at 0.8 µm, only Ti:Sapphire lasers can serve for this aim, as commercially available fiber-coupled spatially multimode AlGaAs laser diodes feature low brightness output. For UC pumping at 1 µm, Yb-fiber lasers benefit from (i) high brightness, (ii) power-scalable output and (iii) optional linear polarization of laser emission. UC pumping drains the population of the metastable Tm^{3+} state preventing unwanted colasing at ~1.9 µm which is detrimental for stable mode-locking.

A Z-shaped astigmatically compensated standing-wave cavity was used, Fig. 4. The laser element was placed between two highly reflective (HR) curved folding mirrors (radius of curvature: RoC = -150 mm). The calculated size (diameter) of the laser mode inside the crystal was 63 × 202 µm^2 (here and below, we specify the mode size for the cavity with an additional intracavity $Tm:LiYF_4$ crystal) in the sagittal and tangential planes, respectively. The pump radiation (pumping into π-polarization) was focused into the crystal through a flat pump mirror (PM) coated for high transmission (HT) at 1.04 µm and HR at 2.15-2.6 µm using an antireflection (AR) coated plano-convex lens (focal length: f = 60 mm). The PM was placed between the crystal and one of the HR curved folding mirrors.

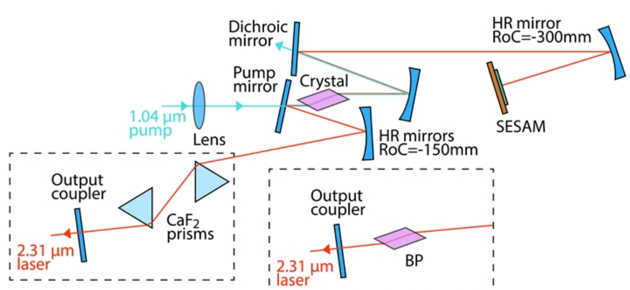

Fig. 4. Scheme of the SESAM mode-locked Thulium laser with upconversion pumping.

One cavity arm contained a dichroic flat folding mirror and a curved HR mirror (RoC = -300 mm) creating a secondary beam waist on the SESAM. The diameter of the laser mode on the SESAM was calculated to be 124 × 246 µm^2 in the sagittal and tangential planes, respectively. The plane dichroic mirror was used to prevent heating the SESAM with the residual non-absorbed pump. Thus, pumping was in single-pass.

The other cavity arm was terminated by a plane-wedged output coupler (OC) with a transmission T_{OC} = 0.5% or 1.5% at the laser wavelength. The HR and dichroic mirrors were coated for HR at 2.2-2.5 µm, HT at 1.04 µm and HT at 1.9 µm (to avoid oscillations on the competitive $^3F_4 \rightarrow {}^3H_6$ Tm^{3+} transition).

Two approaches for the intracavity dispersion management were applied. First, we used a pair of uncoated CaF_2 prisms placed at Brewster's angle in the cavity arm terminated by the OC. The total cavity length was about 1.3 m (0.5% OC) and 1.6 m (1.5% OC). Then, the prisms were removed and an additional passive 6 mm-long Tm:$LiYF_4$ crystal (Brewster plate, BP) was placed at Brewster's angle. It was ***a***-cut and oriented for light polarization π. The group velocity dispersion (GVD) of $LiYF_4$ is -62.69 fs^2/mm at 2.3 µm for *e*-wave [40]. The total geometrical length of the cavity with the BP was about 1.4 m. Tm^{3+} ions do not absorb the laser radiation at 2.3 µm and thus the doping of the available BP does not affect the laser performance.

The laser emission spectra were measured using an optical spectrum analyzer (Yokogawa, AQ6375). The pulse duration was measured using a second harmonic generation (SHG) based autocorrelator (FR-103XL, FEMTOCHROME Research). The radio frequency (RF) spectra were measured using a photodetector (UPD-5N-IR2-P, ALPHALAS, bandwidth: > 0.3 GHz) and an RF spectrum analyzer (R&S FSV7, Rohde & Schwarz).

3.2. Continuous-wave operation

In the continuous-wave (CW) regime (when replacing the SESAM with a plane HR mirror), the laser delivered an output power of 616 mW at 2312-2314 nm with a slope efficiency η of 10.0% (vs. the incident pump power) and a laser threshold of 1.10 W (for T_{OC} = 1.5%), see Fig. 5(a). For smaller T_{OC} of 0.5%, the laser generated 433 mW at 2316 nm with a lower slope efficiency of 7.0% and lower threshold of 0.96 W. The input-output dependences were linear; no signs of detrimental thermal effects were observed. No thermal fracture of the crystal was observed up to at least the maximum applied pump power. Further power scaling was limited by the available pump power.

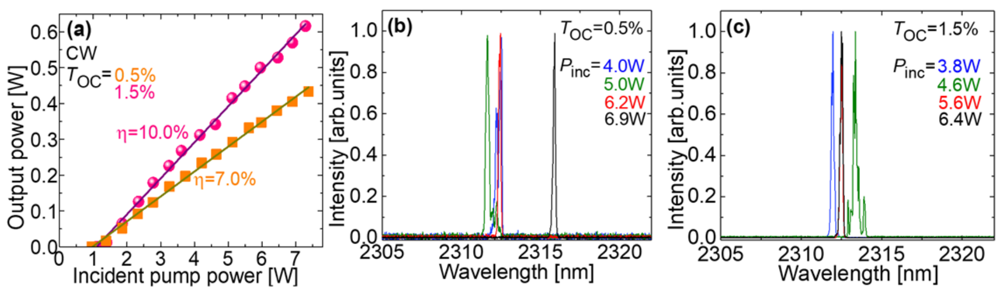

Fig. 5. CW Tm:$LiYF_4$ laser operating on the $^3H_4 \rightarrow {}^3H_5$ transition with upconversion pumping: (a) input-output dependences, η – slope efficiency; (b,c) typical spectra of laser emission: (b) 0.5% OC, (c) 1.5% OC. The laser polarization is π.

The typical laser emission spectra are shown in Fig. 5(b,c). The spectra showed a slight dependence on the pump level and the emission occurred around 2.31 µm (the $^3H_4 \rightarrow {}^3H_5$ Tm^{3+} transition). No unwanted colasing at 1.9 µm was observed.

The developed CW Tm:$LiYF_4$ laser pumped by an Yb-fiber laser represents the record-high power for any upconversion-pumped 2.3 µm Tm laser, cf. Table 2, indicating the high potential of such high-brightness pump sources.

3.3. Passively mode-locked operation

First, the cavity design employing a prism pair for the intracavity dispersion management was studied as it provided more flexibility in varying the group delay dispersion (GDD). For 1.5% OC, upon increasing the incident pump power, the laser passed through CW, passively Q-switched ML (at P_{inc} > 2.2W) and CW ML (at P_{inc} > 2.8 W) operation regimes, Fig. 6(a). For this output coupling, the prism separation was optimized to be 345 mm. The round-trip negative GDD

Optics EXPRESS

Table 2. Performance[a] of 2.3 µm Thulium Lasers with Upconversion Pumping Reported So Far

Crystal	Pump[b]	λ_P, nm	P_{th}, W	P_{out}, mW	η, %	λ_L, µm	Ref.
$Tm:LiYF_4$	TS	1040	0.21	102^{CW}	**14.6**	2.30	[23]
	TS	1055	0.31	46^{CW}	10.9	2.30	[23]
	YFL	1043	1.10	**616^{CW}**	10.0	2.31	This work
$Tm:KY_3F_{10}$	TS	1048	0.34	92^{CW}	14	2.27, 2.33	[14]
	YFL	1064	~0.80	124^{CW}	8	2.34	[26]
$Tm:KLu(WO_4)_2$	YFL	1064	3.19	433^{qCW}	7.4	2.29	[27]

[a] λ_P – pump wavelength, P_{th} – laser threshold, P_{out} – output power, η – slope efficiency vs. incident pump power, λ_L – laser wavelength.
[b] TS – Ti:Sapphire laser, YFL – ytterbium fiber laser; qCW – quasi-CW operation regime.

introduced by the CaF_2 prisms was -2200 fs^2. The SESAM ML Tm-laser delivered a maximum average output power of 450 mW at an incident pump power of 6.44 W, corresponding to an optical efficiency of 7.0%. Assuming a $sech^2$-shaped spectral profile, an emission bandwidth (full width at half maximum, FWHM) of 3.1 nm was obtained at a central wavelength of 2306.5 nm, see Fig. 6(c). The recorded SHG based intensity autocorrelation trace was well fitted with a $sech^2$-shaped temporal intensity profile, yielding an estimated pulse duration of 1.93 ps (FWHM), Fig. 6(e). The corresponding time-bandwidth product (TBP) amounted to 0.337 which was slightly above the Fourier-transform-limit (0.315). The laser operated at a pulse repetition rate of 95.1 MHz.

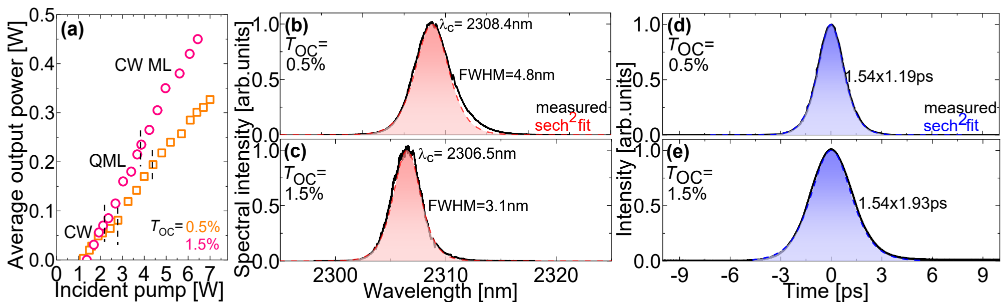

Fig. 6. $Tm:LiYF_4$ laser operating on the $^3H_4 \rightarrow {}^3H_5$ transition passively mode-locked by a GaSb-based SESAM (dispersion management by a prism pair): (a) power transfer characteristics; (b,c) spectra of the mode-locked pulses and (d,e) the corresponding SHG-based intensity autocorrelation traces for output coupler transmission T_{OC} of (b,d) 0.5% and (c,e) 1.5%. *Red* and *blue dashed curves* – $sech^2$ fits. The laser polarization is π.

For smaller T_{OC} of 0.5%, the optimum prism separation was 60 mm. The round-trip negative GDD introduced by the CaF_2 prisms was -650 fs^2. On increasing the pump power, the transitions to passively Q-switched ML and further to CW ML were observed at 2.9 W and 4.4 W, respectively. At the maximum incident pump power of 7.0 W, the average output power from the SESAM ML $Tm:LiYF_4$ laser dropped to 327 mW with an optical efficiency of 4.7%, Fig. 6(a). The CW ML laser operated at the central wavelength of 2308.4 nm with a spectral bandwidth of 4.8 nm (FWHM, for a $sech^2$-shaped spectral intensity profile), see Fig. 6(b). The weak spectral modulation originated from the detection system. Using smaller output coupling allowed us to further shorten the pulse duration: the SHG based intensity autocorrelation measurement yielded a pulse duration of 1.19 ps assuming a $sech^2$-shaped temporal intensity profile, Fig. 6(d). The corresponding TBP of 0.321 was slightly above the Fourier-transform-limit. The measurements of the radio frequency spectra revealed a fundamental beat node at 114.48 MHz with a high extinction ratio of >70 dB above the noise and uniform harmonics over a 1 GHz wide frequency span.

For the laser cavity configuration employing a prism pair for the dispersion management, for both studied OCs, mode-locking was self-starting above the CW ML threshold. Note that the distances between the cavity elements and the total cavity length were slightly different when using 0.5% and 1.5% OCs, and the cavity alignment targeted attaining high mode-locking stability at the expense of somewhat reduced average output power.

The excellent stability of the self-starting mode-locked operation together with the shortest pulse duration were observed when using the BP for the intracavity dispersion management. Its insertion resulted in a total round-trip negative intracavity GDD of -1438 fs^2 at 2310 nm, Fig. 9. When using $T_{OC} = 0.5\%$, on increasing the pump power, the transitions to passively Q-switched ML and further to CW ML operation regimes were observed at the incident pump powers of 2.95 W and 3.96 W, respectively, *i.e.*, the CW ML threshold was reduced as compared to the cavity employing the prism pair. At the incident pump powers above 7.0 W, the CW ML operation required a slight additional cavity adjustment to achieve self-starting behavior. Therefore, the CW ML laser for this cavity design was optimized at a pump power of 6.2 W yielding an average output power of 208 mW and an optical efficiency of 3.4%. The CW ML Tm-laser featured a substantially broader emission spectrum (FWHM: 6.51 nm) at a central wavelength of 2309.4 nm, which enabled us to obtain femtosecond pulses, Fig. 7(a). The background-free SHG based intensity autocorrelation trace was well fitted with the sech^2-shaped profile giving a pulse duration of 870 fs, Fig. 7(b). The corresponding TBP was calculated to be 0.318 just above the Fourier-transform limit. The pulse energy directly generated out of the CW ML Tm:$LiYF_4$ laser amounted to 1.98 nJ. No damage of the SESAM was observed under ML operation.

Typical oscilloscope traces of laser emission from the CW ML laser are shown in Fig. 7(c) ruling out the beating effects. The RF spectra were measured to confirm the stability of the CW ML operation, Fig. 8. The recorded fundamental beat note at 105.08 MHz corresponding to fundamental ML exhibited a high extinction ratio of >80 dB above the noise. The uniform harmonics on a 1-GHz frequency span revealed high stability of the single-pulse mode-locked laser operation without any Q-switching instabilities, see Fig. 8(b). The CW ML operation of the Tm:$LiYF_4$ laser was stable for hours without any degradation of the average output power or the pulse characteristics.

To confirm the proper choice of the dispersion management strategy used in this work, the GDD of the cavity elements and the ideal GDD for the soliton condition were calculated as shown in Fig. 9 for the shortest pulse duration (and lowest TBP) cavity configuration with the intracavity BP. The SESAM is designed to show a simulated GDD profile in the range of 0 – 200 fs^2 over a 60-nm bandwidth near 2310 nm. The total cavity roundtrip GDD accounting for the contributions of the SESAM, the laser crystal and the BP is calculated to be -1438 fs^2 at the center wavelength of the ML laser spectrum. This GDD with considering nonlinear phase shift from the self-phase modulation in the laser gain medium corresponds to an ideal soliton pulse duration limit of 834 fs (FWHM), as calculated using the following equations [21]:

$$\tau_p = 1.76\frac{4|D|}{\delta_{\text{eff}} W}\ , \tag{3a}$$

$$\delta_{eff} = \frac{2\pi}{\lambda}\sum_i \frac{2n_2^i L_i}{A_{eff}^i}, \tag{3b}$$

where τ_{p} is the pulse duration, D is the round-trip GDD, δ_{eff} is the effective nonlinearity coefficient, W is the pulse energy, λ is the laser wavelength, n_2 is the nonlinear refractive index, L is the crystal thickness, and A_{eff} is the effective laser mode area in the crystal (i numbers

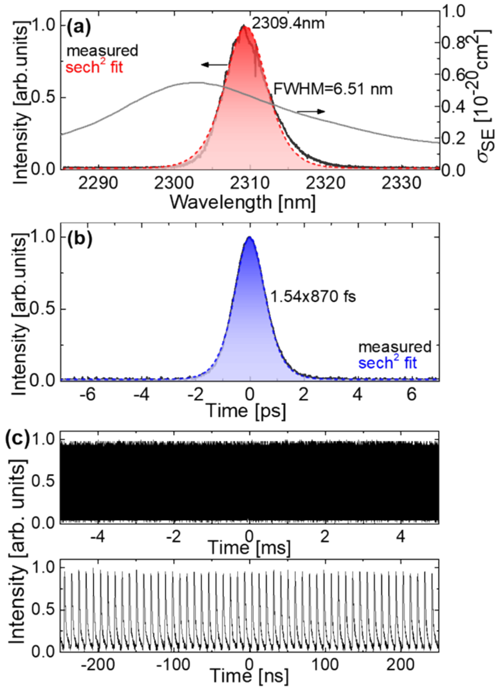

Fig. 7. Characterization of the shortest pulses from the Tm:LiYF$_4$ laser operating on the $^3H_4$ → $^3H_5$ transition passively mode-locked by a GaSb-based SESAM (dispersion management by an intracavity BP): (a) spectrum of the shortest mode-locked pulses, *grey solid curve* – σ_{SE} spectrum for Tm^{3+} ions in LiYF$_4$ (for π-polarized light); (b) the corresponding SHG-based intensity autocorrelation trace, T_{OC} = 0.5%; (c) typical oscilloscope traces of laser emission with different time spans. *Red* and *blue dashed curves* – sech^2 fits. The laser polarization is π.

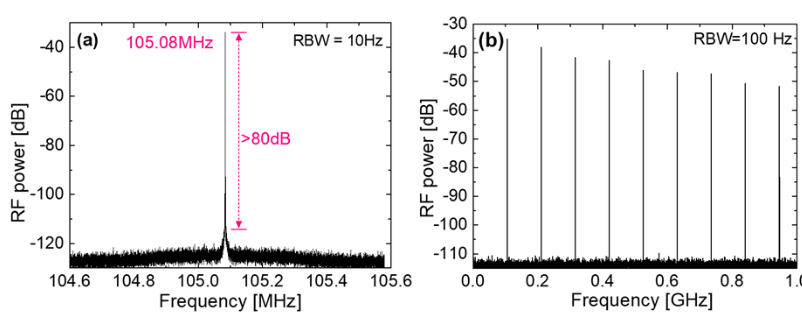

Fig. 8. RF spectra of the SESAM mode-locked Tm:LiYF$_4$ laser operating on the $^3H_4$ → $^3H_5$ transition (dispersion management by an intracavity BP): (a) fundamental beat note recorded with a resolution bandwidth (RBW) of 10 Hz; (b) harmonics on a 1 GHz span, RBW = 100 Hz. T_{OC} = 0.5%.

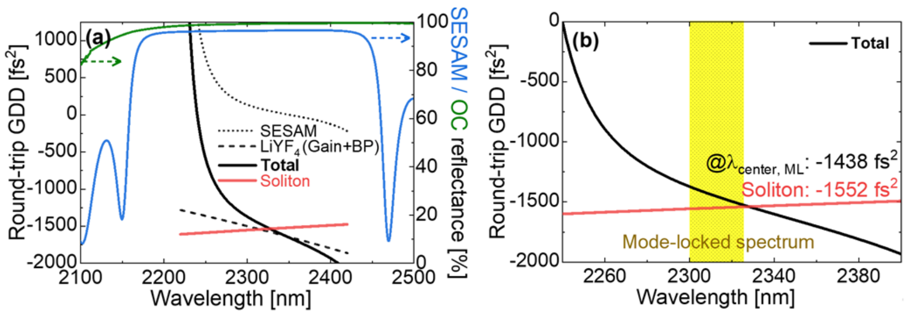

Fig. 9. Dispersion analysis for the SESAM mode-locked $Tm:LiYF_4$ laser operating on the $^3H_4 \rightarrow {}^3H_5$ transition (dispersion management by an intracavity BP): (a) the estimated round-trip GDD of the cavity elements and the measured reflectance curves of the SESAM (*blue solid*) and the OC (*green solid*); (b) a close look on the total round-trip GDD: (a,b) the spectral dependence of GDD: the SESAM (*black dotted*), the $Tm:LiYF_4$ gain crystal, BP (*black dashed*), the total roundtrip cavity GDD (*black solid*). The *red solid* is the GDD needed to satisfy the soliton condition. The *yellow rectangle* marks the range of the mode-locked laser spectrum.

the intracavity crystals, *i.e.*, the laser crystal and the BP). For $LiYF_4$, $n_2 = 1.7 \times 10^{-20}$ m^2/W at ~1.06 µm (polarization-averaged value) [41]. The theoretically required GDD for the observed shortest pulse duration satisfying the soliton condition is -1552 fs^2 at 2310 nm, which agrees well with the dispersion estimation and verifies that our dispersion management using the BP leads to soliton pulse formation. Note that although the $Tm:LiYF_4$ BP can be regarded as an additional Kerr medium, due to the relatively large diameter of the laser mode inside it (calculated value: 3637×1750 μm^2 in the sagittal and tangential planes, respectively), its contribution to the self-phase modulation is almost negligible, namely $\delta_{eff,BP} = 0.002 \times \delta_{eff,gain}$.

The stimulated-emission cross-section, σ_{SE}, spectrum for Tm^{3+} ions in $LiYF_4$ (for light polarization π) is shown in Fig. 7(a). The σ_{SE} value at the central laser wavelength is 0.47×10^{-20} cm^2 and the gain bandwidth (FWHM) is as broad as 25.8 nm indicating a room for further pulse shortening from mode-locked $Tm:LiYF_4$ lasers operating around 2.3 µm, e.g., via Kerr-lens mode-locking.

4. Conclusion

To conclude, we report a significant breakthrough in the development of ultrafast Thulium lasers operating on the $^3H_4 \rightarrow {}^3H_5$ transition around 2.3 µm. This advancement is attributed to two key innovative approaches: (i) the upconversion pumping of bulk, heavily Tm^{3+}-doped crystals using high-brightness, high-power, polarization-maintaining ~1 µm Yb-fiber lasers and (ii) the use of GaSb-based SESAMs. These SESAMs feature wide stopbands, very low non-saturable losses, and fast recovery times, enabling the generation of femtosecond pulses at 2.3 µm. Specifically, by employing a type-I SESAM with a single ternary strained $In_{0.33}Ga_{0.67}Sb$ quantum well embedded in GaSb, we achieved soliton pulse shaping in an upconversion-pumped $Tm:LiYF_4$ laser. This resulted in the generation of soliton pulses as short as 870 fs at the central wavelength of 2309.4 nm with an average output power of 208 mW and a pulse repetition rate of 105.08 MHz. This setup exhibited self-starting mode-locking behavior with excellent stability. Furthermore, we scaled the output power to 450 mW, though at the expense of a longer pulse duration of 1.93 ps. These results represent the first femtosecond SESAM mode-locked Tm-laser at 2.3 µm, and the highest average output power ever extracted from a mode-locked Tm oscillator operating on the $^3H_4 \rightarrow {}^3H_5$ transition. This includes comparisons with lasers employing other saturable absorbers or Kerr-lens mode-locking.

Yb-fiber lasers emitting slightly above 1 µm are expected to boost the performance of Tm-lasers at 2.3 µm. This improvement is expected due to their inherent advantages. These include a commercially developed technology based on silica fibers, a small footprint, high output powers with excellent beam quality, and linearly polarized emission from polarization-maintaining fibers. Additionally, their sufficient wavelength tunability allows for precise addressing of the $^3F_4 \rightarrow {}^3F_{2,3}$ excited-state absorption transition of Tm^{3+} ions. This leads to efficient upconversion pumping driven by the photon avalanche mechanism. In the CW regime, the output power achieved in the present work from the Tm:$LiYF_4$ laser (616 mW at ~2313 nm) sets a new record among all the previously reported upconversion-pumped bulk Tm-lasers at 2.3 µm. This suggests that this approach could be a viable solution for generating watt-level output from such laser sources. This is especially relevant considering the commercial availability of even kW-level single-mode Yb-fiber lasers.

Further pulse shortening is anticipated in mode-locked 2.3-µm Tm-lasers, thanks to the relatively broad gain bandwidth of Tm^{3+}-doped fluoride crystals. These crystals support the generation of sub-250-fs for Tm:$LiYF_4$ and even approximately 100-fs pulses for Tm:KY_3F_{10}. Achieving these pulse durations is expected to involve further optimization of the intracavity dispersion, reduction of the cavity losses through the use of specially designed mirrors, optimizing the crystal quality, or employing Kerr-lens mode-locking. Additionally, a reduction in thermal effects is expected by utilizing upconversion pumping at 1.45 µm with Raman fiber lasers, which address the $^3F_4 \rightarrow {}^3H_4$ excited-state absorption transition of Tm^{3+} ions.

Funding. H2020 Marie Skłodowska-Curie Actions (101034329); Région Normandie (RIN NovaMAT); Agence Nationale de la Recherche (ANR-10-LABX-09-01, ANR-19-CE08-0028); European Regional Development Fund (Chaire RELANCE).

Acknowledgements. We thank FIRST clean room facility at ETH Zurich.

Disclosures. The authors declare no conflicts of interest.

Data availability. Data underlying the results presented in this paper are not publicly available at this time but may be obtained from the authors upon reasonable request.

References

1. F. J. McAleavey, J. O'Gorman, J. F. Donegan, *et al.*, "Narrow linewidth, tunable Tm^{3+}-doped fluoride fiber laser for optical-based hydrocarbon gas sensing," IEEE J. Sel. Top. Quantum Electron. **3**(4), 1103–1111 (1997).
2. M. E. Webber, J. Wang, S. T. Sanders, *et al.*, "In situ combustion measurements of CO, CO_2, H_2O and temperature using diode laser absorption sensors," Proc. Combust. Inst. **28**(1), 407–413 (2000).
3. J. Wang, M. Maiorov, D. S. Baer, *et al.*, "In situ combustion measurements of CO with diode-laser absorption near 2.3 µm," Appl. Opt. **39**(30), 5579–5589 (2000).
4. S. T. Fard, W. Hofmann, P. T. Fard, *et al.*, "Optical absorption glucose measurements using 2.3-µm vertical-cavity semiconductor lasers," IEEE Photonics Technol. Lett. **20**(11), 930–932 (2008).
5. B. Cole, L. Goldberg, S. Chinn, *et al.*, "Compact and efficient mid-IR OPO source pumped by a passively Q-switched Tm:YAP laser," Opt. Lett. **43**(5), 1099–1102 (2018).
6. A. Barh, J. Heidrich, B. O. Alaydin, *et al.*, "Watt-level and sub-100-fs self-starting mode-locked 2.4-µm Cr:ZnS oscillator enabled by GaSb-SESAMs," Opt. Express **29**(4), 5934–5946 (2021).
7. S. Vasilyev, M. Mirov, and V. Gapontsev, "High power Kerr-lens mode-locked femtosecond mid-IR laser with efficient second harmonic generation in polycrystalline Cr2+:ZnS and Cr2+:ZnSe," in *Advanced Solid State Lasers* (Optica Publishing Group, 2014), paper AM3A-3.
8. J. Heidrich, A. Barh, S. L. Camenzind, *et al.*, "Low-noise femtosecond SESAM modelocked diode-pumped Cr:ZnS oscillator," IEEE J. Quantum Electron. **59**(1), 1–7 (2023).
9. E. Geerlings, M. Rattunde, J. Schmitz, *et al.*, "Widely tunable GaSb-based external cavity diode laser emitting around 2.3 µm," IEEE Photonics Technol. Lett. **18**(18), 1913–1915 (2006).
10. G. Boehm, A. Bachmann, J. Rosskopf, *et al.*, "Comparison of InP-and GaSb-based VCSELs emitting at 2.3 µm suitable for carbon monoxide detection," J. Cryst. Growth **323**(1), 442–445 (2011).
11. J. Heidrich, M. Gaulke, M. Golling, *et al.*, "324-fs pulses from a SESAM modelocked backside-cooled 2-µm VECSEL," IEEE Photon. Technol. Lett. **34**(6), 337–340 (2022).
12. J. Caird, L. DeShazer, and J. Nella, "Characteristics of room-temperature 2.3-µm laser emission from Tm^{3+} in YAG and $YAlO_3$," IEEE J. Quantum Electron. **11**(11), 874–881 (1975).

Optics EXPRESS

13. R. Allen and L. Esterowitz, "CW diode pumped 2.3 µm fiber laser," Appl. Phys. Lett. **55**(8), 721–722 (1989).
14. L. Guillemot, P. Loiko, R. Soulard, *et al.*, "Close look on cubic Tm:KY_3F_{10} crystal for highly efficient lasing on the $^3H_4 \rightarrow {}^3H_5$ transition," Opt. Express **28**(3), 3451–3463 (2020).
15. P. Loiko, R. Soulard, L. Guillemot, *et al.*, "Efficient Tm:$LiYF_4$ Lasers at ~2.3 µm: Effect of Energy-Transfer Upconversion," IEEE J. Quantum Electron. **55**(6), 1–12 (2019).
16. P. Loiko, E. Kifle, L. Guillemot, *et al.*, "Highly efficient 2.3 µm thulium lasers based on a high-phonon-energy crystal: evidence of vibronic-assisted emissions," J. Opt. Soc. Am. B **38**(2), 482–495 (2021).
17. J. F. Pinto, L. Esterowitz, and G. H. Rosenblatt, "Tm^{3+}:YLF laser continuously tunable between 2.20 and 2.46 µm," Opt. Lett. **19**(12), 883–885 (1994).
18. X. Yu, K. Eremeev, Z. Pan, *et al.*, "Six-watt diode-pumped Tm:$GdVO_4$ laser at 2.29 µm," Opt. Lett. **48**(24), 6404–6407 (2023).
19. R. Soulard, A. Tyazhev, J.-L. Doualan, *et al.*, "2.3 µm Tm^{3+}:YLF mode-locked laser," Opt. Lett. **42**(18), 3534–3536 (2017).
20. M. Kowalczyk, L. Guillemot, P. Loiko, *et al.*, "SESAM-mode-locked Tm:KY3F10 laser at 2340 nm," in *Laser Congress 2020 (ASSL, LAC)* (Optica Publishing Group, 2020), paper JTh2A.15.
21. F. Canbaz, I. Yorulmaz, and A. Sennaroglu, "Kerr-lens mode-locked 2.3-µm Tm^{3+}:YLF laser as a source of femtosecond pulses in the mid-infrared," Opt. Lett. **42**(19), 3964–3967 (2017).
22. A. Muti, F. Canbaz, M. Tonelli, *et al.*, "Graphene mode-locked operation of Tm^{3+}:$YLiF_4$ and Tm^{3+}:KY_3F_{10} lasers near 2.3 µm," Opt. Lett. **45**(3), 656–659 (2020).
23. L. Guillemot, P. Loiko, R. Soulard, *et al.*, "Thulium laser at ~2.3 µm based on upconversion pumping," Opt. Lett. **44**(16), 4071–4074 (2019).
24. M. F. Joubert, S. Guy, and B. Jacquier, "Model of the photon-avalanche effect," Phys. Rev. B **48**(14), 10031–10037 (1993).
25. A. Tyazhev, F. Starecki, S. Cozic, *et al.*, "Watt-level efficient 2.3 µm thulium fluoride fiber laser," Opt. Lett. **45**(20), 5788–5791 (2020).
26. Y. Morova, M. Tonelli, V. Petrov, *et al.*, "Upconversion pumping of a 2.3 µm Tm^{3+}:KY_3F_{10} laser with a 1064 nm ytterbium fiber laser," Opt. Lett. **45**(4), 931–934 (2020).
27. A. Tyazhev, P. Loiko, L. Guillemot, *et al.*, "Excited-state absorption and upconversion pumping of Tm^{3+}-doped potassium lutetium double tungstate," Opt. Express **31**(9), 14808–14820 (2023).
28. H. Dupont, P. Loiko, A. Tyazhev, *et al.*, "Tm:CALGO lasers at 2.32 µm: cascade lasing and upconversion pumping," Opt. Express **31**(12), 18751–18764 (2023).
29. H. Dupont, L. Guillemot, P. Loiko, *et al.*, "Dual-wavelength-pumping of mid-infrared Tm:YLF laser at 2.3 µm: demonstration of pump seeding and recycling processes," Opt. Express **30**(18), 32141–32150 (2022).
30. U. Keller, K. J. Weingarten, F. X. Kärtner, *et al.*, "Semiconductor saturable absorber mirrors (SESAM's) for femtosecond to nanosecond pulse generation in solid-state lasers," IEEE J. Sel. Top. Quantum Electron. **2**(3), 435–453 (1996).
31. C. Hönninger, R. Paschotta, F. Morier-Genoud, *et al.*, "Q-switching stability limits of continuous-wave passive mode locking," J. Opt. Soc. Am. B **16**(1), 46–56 (1999).
32. B. Ö. Alaydin, M. Gaulke, J. Heidrich, *et al.*, "Bandgap engineering, monolithic growth, and operation parameters of GaSb-based SESAMs in the 2–2.4 µm range," Opt. Mater. Express **12**(6), 2382–2394 (2022).
33. J. Paajaste, S. Suomalainen, R. Koskinen, *et al.*, "GaSb-based semiconductor saturable absorber mirrors for mode-locking 2 µm semiconductor disk lasers," Phys. Status Solidi C **9**(2), 294–297 (2012).
34. L. Wang, W. Chen, Y. Zhao, *et al.*, "Sub-50 fs pulse generation from a SESAM mode-locked Tm,Ho-codoped calcium aluminate laser," Opt. Lett. **46**(11), 2642–2645 (2021).
35. Y. Wang, P. Loiko, Y. Zhao, *et al.*, "Polarized spectroscopy and SESAM mode-locking of Tm,Ho:CALGO," Opt. Express **30**(5), 7883–7893 (2022).
36. A. Barh, A. Nussbaum-Lapping, J. Heidrich, *et al.*, "Single-cavity dual-modelocked 2.36-µm laser," Opt. Express **31**(4), 6475–6483 (2023).
37. J. Heidrich, M. Gaulke, B. O. Alaydin, *et al.*, "Full optical SESAM characterization methods in the 1.9 to 3-µm wavelength regime," Opt. Express **29**(5), 6647–6656 (2021).
38. F. X. Kärtner, I. D. Jung, and U. Keller, "Soliton mode-locking with saturable absorbers," IEEE J. Sel. Top. Quantum Electron. **2**(3), 540–556 (1996).
39. I. D. Jung, F. X. Kärtner, L. R. Brovelli, *et al.*, "Experimental verification of soliton mode locking using only a slow saturable absorber," Opt. Lett. **20**(18), 1892–1894 (1995).
40. N. P. Barnes and D. J. Gettemy, "Temperature variation of the refractive indices of yttrium lithium fluoride," J. Opt. Soc. Am. **70**(10), 1244–1247 (1980).
41. D. Milam, M. J. Weber, and A. J. Glass, "Nonlinear refractive index of fluoride crystals," Appl. Phys. Lett. **31**(12), 822–825 (1977).